JTTEE5 7:340-348

Thermal Shock Testing of Burner Cans Coated with a Thick Thermal Barrier Coating

P. Bengtsson, T. Ericsson, and J. Wigren

(Submitted 18 December 1997; in revised form 30 March 1998)

Thick (1.8 mm) thermal barrier coatings were air-plasma-sprayed onto two different substrate geometries, including small circular substrates and burner cans. Two different top-coating spray parameters were used, where the settings of the substrate temperature and the lamella thickness were varied. A segmentation crack network was found in the top coatings sprayed using a high substrate temperature and a high lamella thickness. The density of segmentation cracks was found to be independent of substrate geometry. No segmentation cracks were found in the top-coatings when a low substrate temperature and a low lamella thickness were used.

In the segmented burner can, after 1000 thermal shock cycles, the segmentation crack network was still stable and no severe cracks had formed in the top coating. In the nonsegmented burner can, cracks were formed after only 35 thermal shock cycles. Among the crack types, horizontally oriented cracks were found in the top coating close to, and sometimes reaching, the bond coating. Cracks of this type are not tolerated in thermal barrier coatings because they can cause failure of the coating.

Regarding the lifetime of the segmented burner can, it is believed the failure will be dependent on other mechanisms, such as bond-coating oxidation or top-coating decomposition.

Keywords	burner can, segmentation crack, thermal barrier coating, thermal shock, zirconia

1. Introduction

The demand for lower exhaust emissions within the jet engine industry has led to the development of new combustion techniques. The techniques include lean premixed prevaporized (LPP) concepts, where prevaporization of the fuel and premixing of the vaporized fuel with compressed air are done before combustion occurs. This gives a very homogeneous fuel-air mixture and a uniform temperature distribution within the combustor. In order to further keep the combustion temperature within a tight interval, film cooling of the inside of the combustor wall is not used. The objective with combustion in a narrow and optimized temperature interval is to keep the amounts of emission species at a low level. High combustion temperatures produce a large amount of NO_x, while low combustion temperatures promote the formation of CO and HC.

The absence of film cooling on the combustor walls requires materials which can operate at higher temperatures. This trend is also present for conventional diffusion combustors, where higher combustion temperatures are sought as a way to increase the fuel efficiency of the jet engine (Ref 1). One way to meet the requirements is to apply insulating thermal barrier coatings (TBCs) onto the burner can wall. The coatings usually consist of an MCrAlY bond coating and a partially stabilized ZrO_2 top-coating. The thicker the top coatings, the better the insulation of the underlying substrate material. On the other hand, for a given heat flow, a thicker top coating not only lowers the substrate temperature, but also results in a higher top-coating surface temperature. Too high a temperature can cause detrimental phase transformations within the top coating (Ref 2), and this must therefore be considered in the engineering phase.

Few articles have been published regarding thick TBCs, but Johner et al. (Ref 3) sprayed a very thick (5 mm) TBC onto the inside of a superalloy ring. A segmentation crack network was found within the top coating. The ring was thermally shock tested in a flame rig where the highest gas temperature reached 1000 °C. No separation between the coating and the substrate material was found. The authors claimed the good thermal shock resistance to be dependent on the favorable segmentation crack network. Nerz et al. (Ref 4) and Taylor et al. (Ref 5) studied the thermal shock behavior of flat substrates coated with 1.3 mm thick TBCs. The results indicate that the thermal shock resistance of the samples is improved if the top coatings contain a segmentation crack network. Taylor also studied thermal properties such as thermal diffusivity and thermal conductivity of thick TBCs (Ref 6). The properties were found to increase slightly at high-temperature exposure, probably due to healing of horizontally oriented microcracks. Wang et al. reported a 40% increase in thermal shock life time when 1.5 mm thick laser-glazed TBCs were tested and compared to nonglazed samples (Ref 7). The laser glazing produced segmentation cracks in the top coatings. A patent regarding improved thermal shock resistance of TBCs, by incorporating top-coating segmentation cracks, has also been published (Ref 8).

P. Bengtsson, Volvo Aero Corporation (presently at Department of Mechanical Engineering, Division of Engineering Materials, Linköping University, S-581 83 Linköping, Sweden); **T. Ericsson,** Division of Engineering Materials, Department of Mechanical Engineering, Linköping University, S-581 83 Linköping, Sweden; and **J. Wigren,** Volvo Aero Corporation, Surface Technology, 461 81 Trollhättan, Sweden. Contact P. Bengtsson at e-mail: vac.prbn@memo.volvo.se.

The objective of this study is to investigate the thermal shock behavior of an LPP burner can that has been coated with a plasma-sprayed thick thermal barrier coating. Following the conclusions from the literature (Ref 3-5, 7), a burner can with a segmented top coating is compared to a burner can with a non-segmented top coating. The study focuses not only on crack propagation during the testing, but also on other time-dependent mechanisms, such as oxidation and phase transformation. Because most of the coating development is performed with small test substrates instead of real components, coating differences depending on the substrate geometry are also studied.

2. Experimental Details

2.1 Materials

The TBCs, composed of a bond coating and a top coating, were air-plasma-sprayed onto a nickel-base alloy, Hastelloy X (Stoody Deloro Stellite, Inc., Industry, CA). A Praxair NI-171 (Praxair Inc., Danbury, CT) powder was used for the bond coating. The powder was gas-atomized with a chemical composition of 47Ni-23Co-17Cr-12.5Al-0.5Y wt%, and a powder size of 38 to 75 μm. The top-coating powder was Amperit 827.090, manufactured by H.C. Starck Inc., Newton, MA. The powder was agglomerated and sintered with chemical composition $92ZrO_2$-$8Y_2O_3$ wt%, and a powder size of 10 to 106 μm.

2.2 Spraying Details

Circular substrate. Small, circular substrates with a diameter of 25 mm and a thickness of 6 mm were grit-blasted on the flat surface to be coated. The grit-blasted substrates were inserted in holes on the wall of a fixture (Fig. 1a). The fixture was attached to a turntable which, during spraying, rotated around its axis. A Sulzer Metco F1 extension gun (Sulzer-Metco, Westbury, NY), operating at 20 kW, was used for the deposition of both the bond coating and the top coating. The plasma gun moved up and down in the vertical direction, with each passage depositing a thin layer of molten material on the rotating substrates. The coating material resulting from one passage of the plasma gun is called a "lamella." During the spraying, the substrate temperature was monitored with a thermocouple located in one of the substrates, 0.5 mm below the grit-blasted surface. The bond coating was sprayed to a total thickness of 0.16 mm, employing ten passages of the plasma gun.

Two sets of samples, CS1 and CS2, were produced by using different top-coating spray parameters (Table 1). Other spray parameters were kept constant for the two spray sets. The top coatings were sprayed to a total thickness of 1.8 mm.

Before spraying the top coatings, the bond-coated substrates were preheated to their respective substrate temperatures. This was done by directing the plasma torch without any powder feed, toward the bond-coated substrates. During the spraying, the substrate temperature was controlled by using different amounts of cooling. Air jets, attached to the plasma gun and directed parallel to the plasma torch, were used during the spraying of CS1. The pressure of the air was 4.8 bar. No cooling was used during the spraying of CS2. The thickness of the lamellae was controlled by the velocity of the plasma gun—a low velocity giving thicker lamellae.

Burner can geometry. A bond coating and a top coating were plasma-sprayed onto the inside of the burner cans (Fig.

Table 1 Differences in top-coating spray parameters for the circular substrates (CS)

Spray set	Substrate temperature, °C	Lamella thickness, μm
CS1 (cold sprayed)	70	11
CS2 (hot sprayed)	360	41

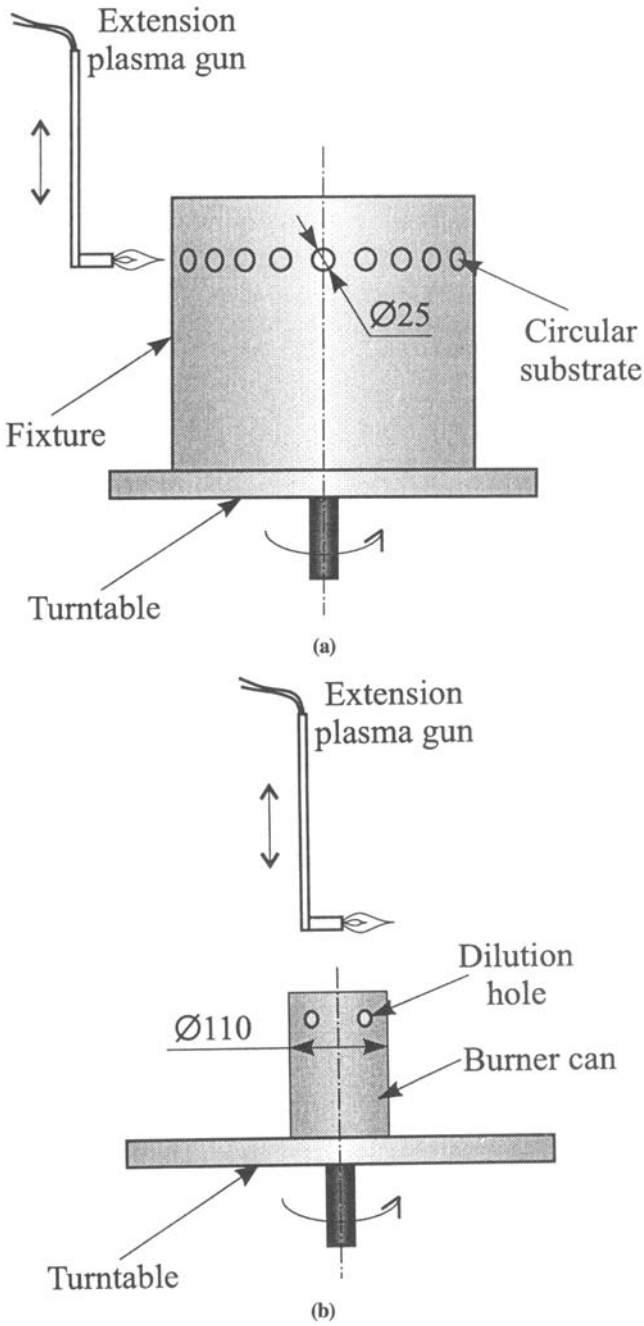

Fig. 1 Setup for the spraying of (a) cylindrical substrates and (b) burner cans

1b). The cans had a diameter of 110 mm, a length of 175 mm, and a wall thickness of 1.2 mm. Each can was mounted to the same turntable that was used for the circular substrates, and the same extension gun was used for the spraying. The substrate temperature was measured with a pyrometer (Impac IN5, Impac Electronics GmbH, Frankfurt, Germany; 0 to 700°, emissivity set to 0.8) that was directed toward the outside of the burner can. The bond coating was sprayed in the same manner as for the circular substrates.

Two sets of cans were sprayed. The top-coating spray conditions were intended to be the same as those used for the circular substrates. Table 2 shows the achieved substrate temperature and lamella thickness. Other spray parameters were the same as those used for the circular substrates. The bond-coated substrates were preheated, and the total top-coating thickness was 1.8 mm. Two burner cans were sprayed for each spray set; one burner can was used for thermal shock testing, and the other for microstructural studies of the as-sprayed structure.

Table 2 Differences in top-coating spray parameters for the burner cans

Burner can	Substrate temperature, °C	Lamella thickness, μm
BC1 (cold sprayed)	100	10
BC2 (hot sprayed)	370	38

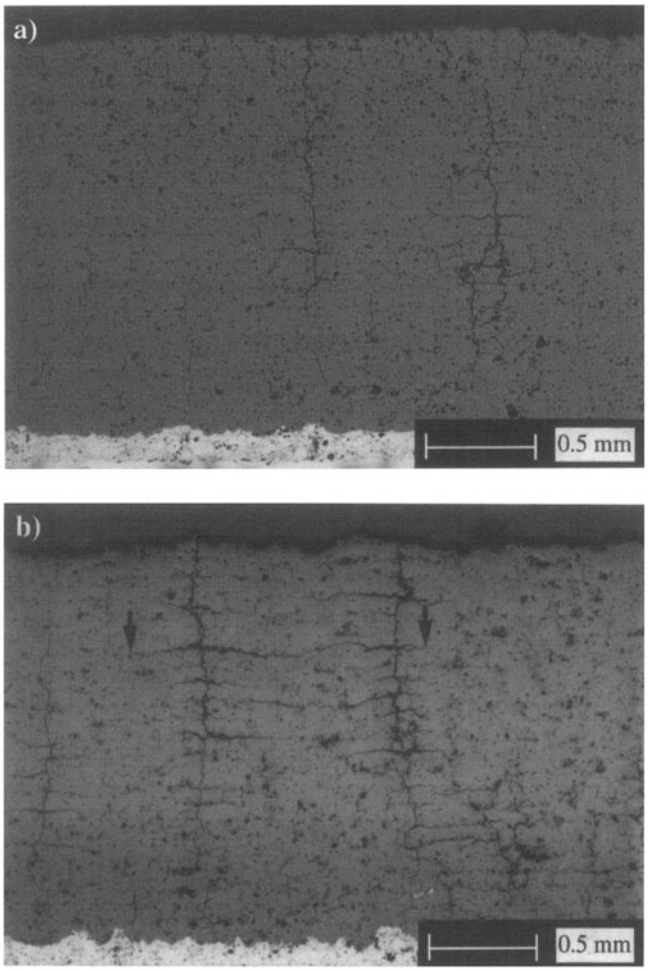

Fig. 2 Polished cross sections of (a) CS2 and (b) BC2. Vertically oriented segmentation cracks and horizontally oriented branching cracks are visible. The length of the longest branching crack found in (b) is measured as the horizontal distance between the arrows in the figure.

2.3 Microstructural Evaluation

Pieces measuring 3 by 3 cm were cut from three positions (bottom, middle, and top) of the burner cans. The bottom position was located between the dilution holes and the closest burner can end, whereas the top position was located at the other end of the burner can. The pieces, together with the circular substrates, were vacuum-impregnated with epoxy, allowing the epoxy to penetrate cracks and pores within the top coating. The molded samples were cut and polished to both cross sections and planar sections of the top coatings. Vertically oriented cracks with a length exceeding half the top-coating thickness were found in the hot-sprayed samples (Fig. 2). The cracks were named "segmentation cracks." To quantify the segmentation cracks in each spray set, a segmentation crack density value was calculated. The density was obtained by dividing the number of segmentation cracks found in a cross section by the horizontal length of the cross section examined. The unit of density corresponds to mm^{-1}. The error associated with the density determinations was estimated to be at most 15% of the measured value. This error takes into account the uncertainty of deciding if a crack is a segmentation crack or not. Horizontally oriented branching cracks were found to accompany the segmentation cracks, (Fig. 2). The length of a branching crack was defined as the horizontal distance between the ends of the crack. The average value of the three longest branching cracks found for each cross section was taken as a measure of the branching crack length.

Radiography was used as a nondestructive tool to visualize the segmentation crack network in the burner cans, both before and after thermal shock testing. An x-ray source was positioned against the exterior of the burner can and photographic film was placed against the coating on the interior of the can. A Philips MCN161 (Philips, Eindhoven, Holland) equipment piece running at 160 kV was used for the radiography tests. Photographs were taken around the whole can to show its complete structure.

2.4 Thermal Shock Testing

Thermal shock testing of the burner cans was performed in a rig, based on the LPP combustion technique. One thermal shock cycle consisted of an 85 s heating period followed by a 75 s cooling period. The wall temperatures of the burner cans were measured with five thermocouples attached to the outside of the wall, positioned from the bottom to the top of the can (Fig. 3). Repeated inspections of the cans were made during testing, in order to optically detect possible failures or flaws of the coatings.

2.5 Phase Analysis

X-ray diffraction phase analyses of the top coatings were performed on the burner cans before and after thermal shock testing. The phase analyses were done on the surface of the top-coatings at a position 30 mm below the upper end of the can, at the same location as thermocouple TC5 during thermal shock

testing (Fig. 3). The diffraction measurements were performed using a Seifert diffractometer (Rich. Seifert and Co, Ahrensburg, Germany) with Cu K_α radiation. A monochromator was positioned on the diffracted beam, and a scintillation detector was used for the x-ray detection. The diffraction angles for the $(11\bar{1})$ monoclinic phase, the (111) tetragonal phase, and the (111) monoclinic phase were all found in the 2θ range between 27.7 and 32.0°. The integrated intensities of the diffracted peaks were determined by least-squares fitting of pseudo-Voigt functions to the measured peaks (Ref 9). Following Toraya et al. (Ref 10), the monoclinic volume fraction, V_m, was calculated from

$$V_m = \frac{P \cdot X_m}{1 + (P - 1) \cdot X_m} \quad \text{(Eq 1)}$$

where the value of P was calculated by Toraya et al., for the present composition, as 1.3 (Ref 11). For a monoclinic-tetragonal system, X_m is the integrated intensity ratio defined by

$$X_m = \frac{I_m(11\bar{1}) + I_m(111)}{I_m(11\bar{1}) + I_m(111) + I_{T'}(111)} \quad \text{(Eq 2)}$$

where I is the integrated intensity from the monoclinic (m) and tetragonal (T′) phases.

3. Results and Discussion

3.1 Microstructural Comparison, Cylindrical Substrates/Burner Cans

Several authors state that the thermal shock life of thick TBCs is considerably increased if the top coatings contain a segmentation crack network (Ref 3-5). At Volvo Aero Corporation, several studies of segmentation cracks have been performed on coatings sprayed onto circular substrates. Real components are usually larger, and there is an interest in evaluating possible differences between the cylindrical test substrates and real components, such as burner cans. The microstructural evaluation is based on the most important features for the thermal shock life, namely segmentation crack density and the adjoining branching cracks.

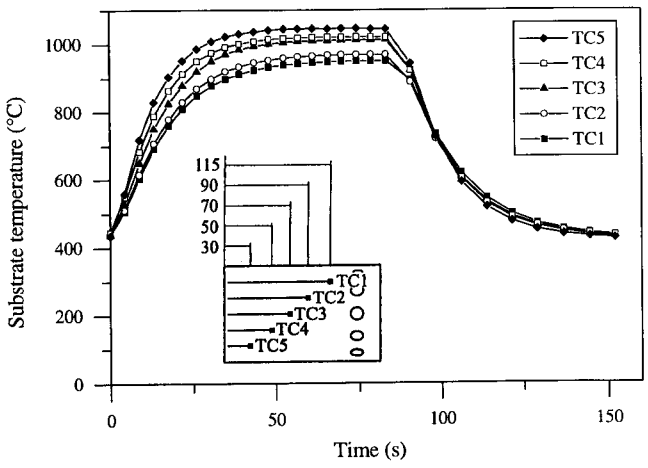

Fig. 3 Measured substrate temperatures during a thermal shock cycle. The thermocouples are positioned on the outside of the burner can; thermocouple 5 at the upper position close to the combustion center, and thermocouple 1 close to the diffusion holes.

Segmentation Crack Density. Figure 4 shows polished planar sections of the hot-sprayed cylindrical substrate, CS2, and the corresponding as-sprayed burner can, BC2. It can be seen that both samples contain a segmentation crack network. The segmentation cracks surround approximately circular segments of top-coating material with a diameter of ~1.8 mm. Thinner cracks, within the segments, can also be seen at some locations. The segmentation crack densities were measured on polished cross sections (Fig. 2). Table 3 shows the measured densities from the circular substrates and the burner cans. No segmentation cracks were visible in the cold-sprayed samples, CS1 and BC1.

The measured segmentation crack density values at the different positions within BC2 were found to be similar, indicating the presence of a consistent crack network throughout the entire burner can. This was verified by the radiography experiments, where the segmentation crack network was clearly seen. The

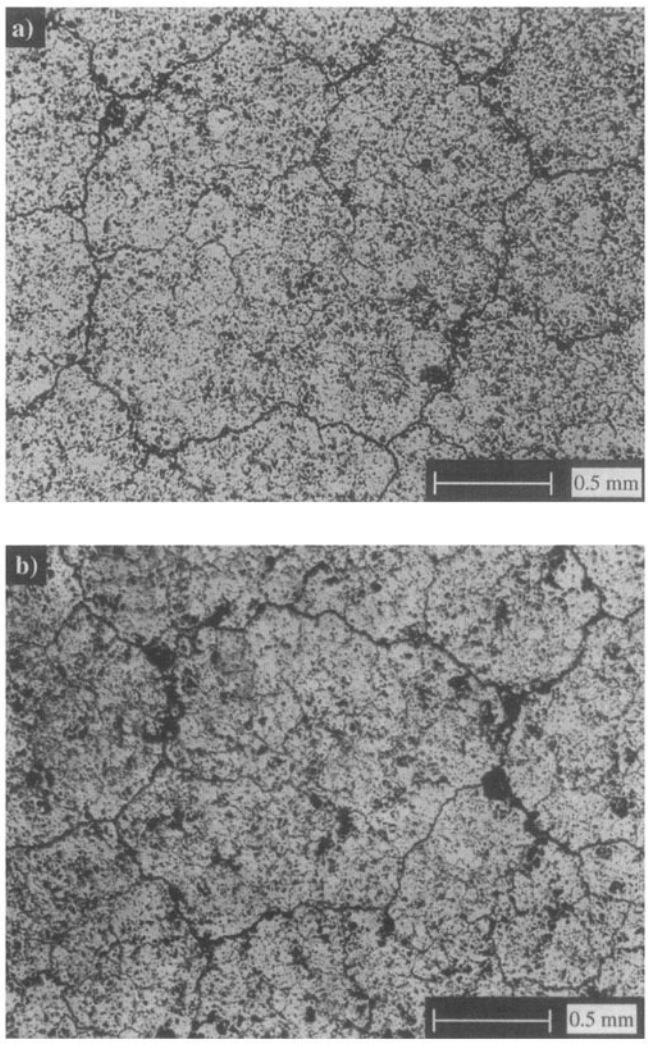

Fig. 4 Polished planar sections of (a) CS2 and (b) BC2. A segmentation crack network is distinguishable in the top coatings.

segmentation crack density value found in CS2 was slightly lower, but considering the error associated with the measurements, the difference is not significant. Note, too, that spraying with a high-substrate temperature and a high-passage thickness, using an extension plasma gun, gave a segmentation crack network. This observation was found in an earlier investigation, where segmentation cracks were studied in top coatings sprayed with a Plasma-Technik F4 gun (Sulzer-Metco, Westbury, NY) (Ref 12).

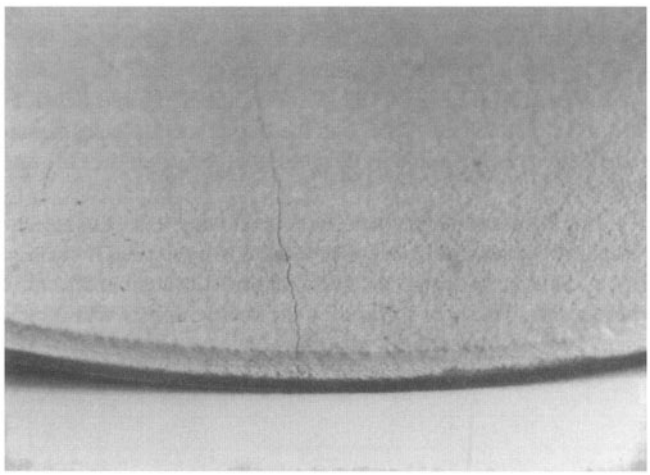

Fig. 5 A vertically oriented crack, visible in BC1 after 35 thermal shock cycles. The top-coating thickness is 1.8 mm.

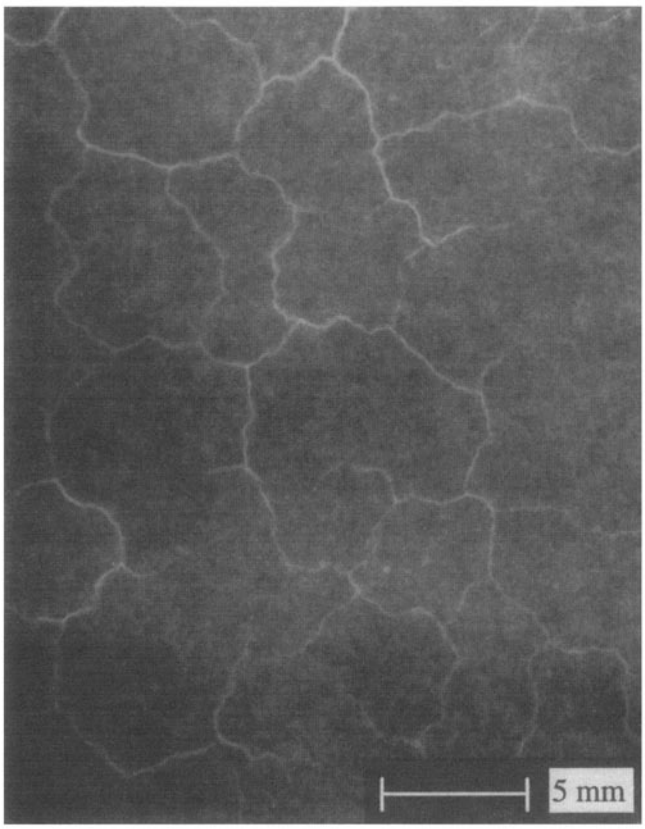

Fig. 6 Radiography photo of BC1 after 35 thermal shock cycles. The photo is taken at the upper position, at the same location as thermocouple TC5.

Branching Crack Length. Horizontally oriented branching cracks are seen to originate from the segmentation cracks, as shown in the polished cross sections of CS2 and BC2 in Fig. 2. The average values of the three longest branching cracks for each cross section are presented in Table 3. The values indicate that the branching crack length is similar within the burner can. Note, too, that the longest branching cracks pass several segmentation cracks before they end. The branching crack length in CS2 is significantly shorter than the observed lengths in BC2. No clear explanation of the difference has been found, but it is noticed that the substrate geometry affects the branching crack length.

3.2 Burner Can Thermal Shock Life

Test Conditions. The measured substrate temperatures during a thermal shock cycle are shown in Fig. 3. The maximum temperature is found at the end of the heating period at the top position of the burner can, where the substrate temperature reaches 1030 °C (indicated by thermocouple TC5). Lower substrate temperatures are found toward the bottom position of the burner can. From a static heat transfer analysis, the maximum top-coating temperature difference is estimated to reach 400 °C, indicating a top-coating surface temperature of 1400 °C (Ref 13). At the end of the cooling period, a substrate temperature of 430 °C was reached. Apart from the thermal cycling of the material, the pressure in the burner can varies during the thermal shock cycle. During the heating period, a pressure of 5 bar exists, whereas during the cooling period, the pressure decreases to 3 bar.

Defect Studies. Visual inspections of BC1 (the cold-sprayed burner can) were made after 5, 15, and 35 thermal shock cycles. After 35 cycles, top-coating cracks could be seen on the edge at the top position of the burner can, extending in the axial direction as shown in Fig. 5. The cracks extended about 20 mm in the axial direction, where they appeared to end. Similar cracks could be seen to originate from the dilution holes. The cracks were regularly spaced around the edge of the hole and extended in a direction normal to the free surface of the hole. At this point, the thermal shock test was terminated.

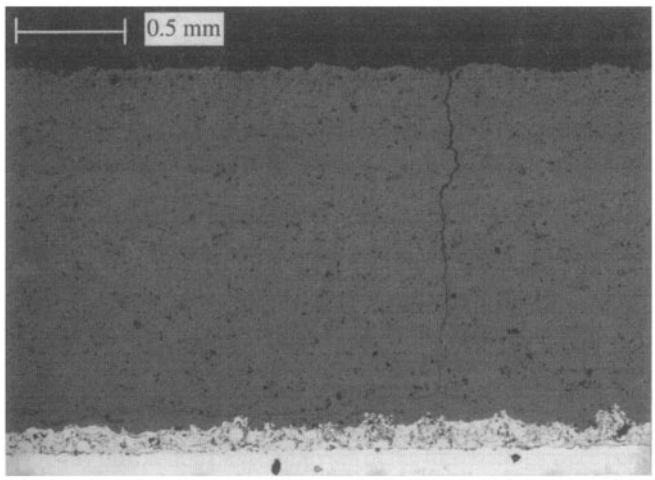

Fig. 7 Polished cross section of BC1 after 35 thermal shock cycles. The photo is taken from the middle position of the burner can. A detrimental horizontal crack is seen just above the bond-coating/top-coating interface.

The radiography examination of the burner can wall showed the existence of a crack network in the remainder of the burner can top-coating (Fig. 6). The crack network resembles the segmentation crack network found in BC2, with the difference that a more coarse-meshed crack network is found in the thermally shocked BC1. Two more differences are found when cross sections of the top coatings are studied. First, the crack network found in BC1 does not contain any branching cracks (Fig. 7). Second, the vertical crack in Fig. 7 is linked to a horizontal crack, which propagates in the top coating close to, and sometimes touching, the bond coating. This type of horizontal crack was found at all three positions examined in the thermally shocked BC1. In fact, a horizontal crack was visible to the naked eye at the top-coating/bond-coating interface at one of the dilution holes. From a polished cross section, the horizontal crack was found to extend from the dilution hole ~8 mm in the axial direction. The development of horizontal cracks at the interface between the top coating and bond coating cannot be allowed in TBCs. On cylindrical substrates, it has been shown that TBC systems fail by the propagation of a horizontal crack at the interface; eventually, the top coating falls off from the underlying material (Ref 14, 15).

Thermal shock testing of BC2 (the hot-sprayed burner can) was performed until 1000 cycles were reached. At this time, the test was terminated because allowable test-rig time was exceeded. The visual inspections of the burner can during testing did not reveal any top-coating changes. This is further demonstrated by comparing radiography photos taken on a BC2 can

Table 3 Measured densities of segmentation cracks and branching crack lengths in as-sprayed samples, and after thermal shock testing

Sample	As-sprayed segmentation crack density, mm^{-1}	As-sprayed branching crack length, mm	Segmentation crack density after thermal shock, mm^{-1}	Branching crack length after thermal shock, mm
CS1	0	0	...	...
CS2	1.31	0.6	...	...
BC1	0	0	0	0
BC2—top position	1.43	1.6	1.22	2.3
BC2—middle position	1.45	1.6	1.40	1.9
BC2—bottom position	1.38	1.8	1.40	1.8

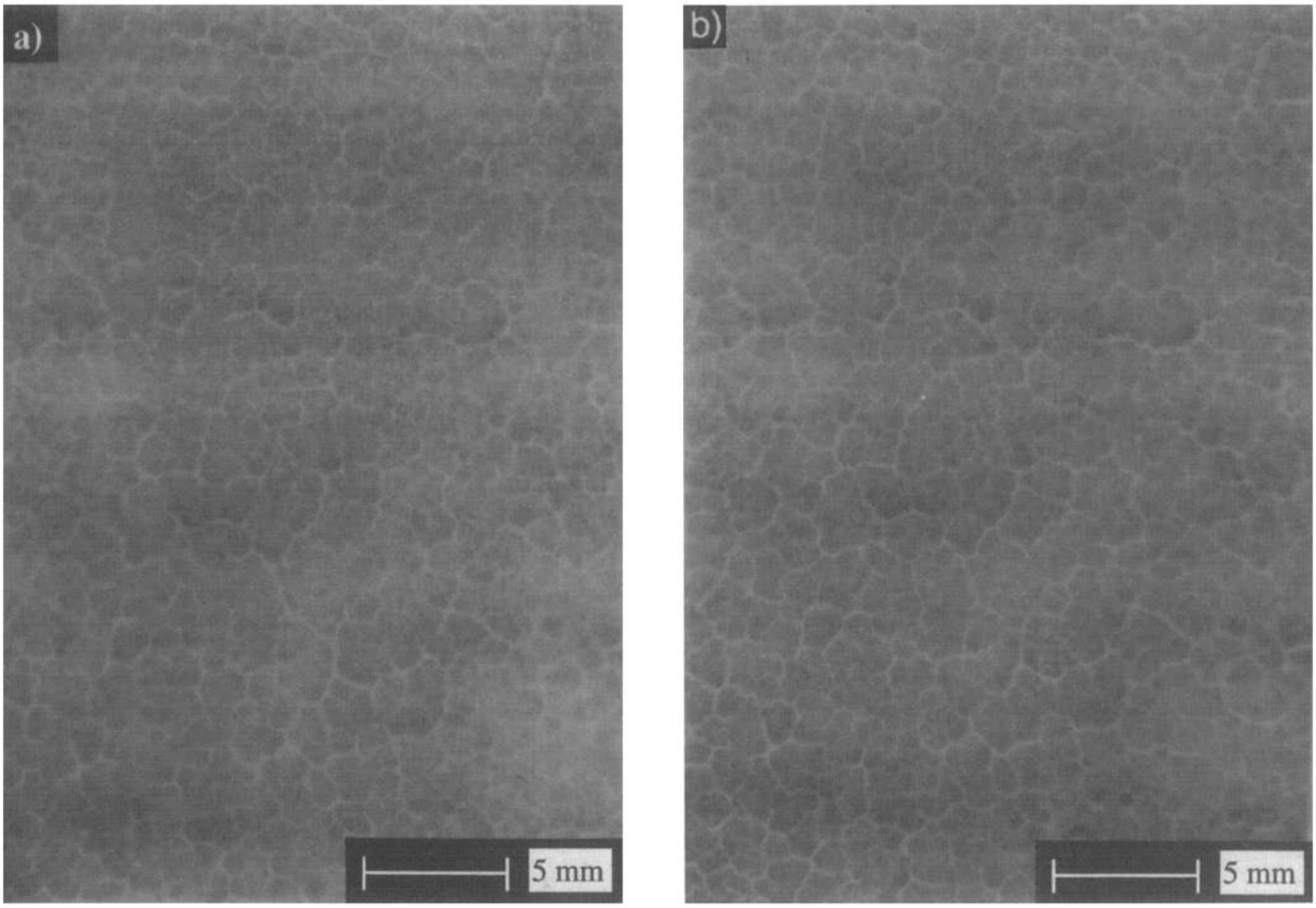

Fig. 8 Radiography photos of BC2 taken from the upper position, same location as thermocouple TC5, (a) before thermal shock testing and (b) after thermal shock testing

before the thermal shock test, to photos taken *after* the test (Fig. 8). The segmentation crack network after testing was identical to the network in the as-sprayed condition. The observation that no new segmentation cracks were created during the thermal shock test was verified with measurements of segmentation crack densities after thermal shock testing, as shown in Table 3. (Note that two BC2 cans were made: one for as-sprayed microstructural investigations, and one for thermal shock testing). Table 3 also shows the measured branching crack lengths of BC2 after the thermal shock testing. Slightly longer cracks (20%) were found in the thermally shocked burner can, which indicates a propagation of the cracks during the testing.

A comparison between the segmented burner can (BC2) and the nonsegmented burner can (BC1) shows that BC2 has a much more stable structure regarding crack propagation during thermal shock testing. The most important difference concerns the initiation and propagation of the horizontal cracks at the interface between the top-coating and the bond coating. These cracks are found in the nonsegmented burner can after the thermal shock test, in contradistinction to the segmented burner can where no such cracks are visible. As the burner can is heated, stresses in the coating and in the substrate will develop because of the difference in thermal expansion coefficients between the materials. At free edges, such as at the ends of the cans and around the segmentation cracks, shear stresses at the interface between the coating and the substrate will develop. The magnitudes of the shear stresses are dependent on the area between the coating and the substrate. Smaller shear stresses are found when the area is small, similar to the shear lag model for composite materials (Ref 16). Therefore, smaller shear stresses are found in a segmented burner can, and the driving force to produce an interface crack is reduced.

Top-Coating Phase Stability. The room-temperature equilibrium phases in a mixture of zirconia, partially stabilized with 8 wt% yttria, are expected to be a monoclinic phase with a low yttria content, m, and an yttria-rich cubic phase, c (Ref 17). However, the rapid cooling of the top-coating material during the plasma-spraying process gives a nonequilibrium tetragonal phase, denoted T′. This phase is referred to as nontransformable because it does not transform into the monoclinic phase during the rapid cooling after spraying (Ref 18). Nevertheless, the T′ phase is known to decompose into a low-yttria tetragonal phase, t, and the yttria-rich cubic phase when it is annealed at high temperatures. After the anneal, during cooling to room temperature, the tetragonal phase, t, transforms to the monoclinic phase, m. This transformation (t to m) is associated with a volume expansion of ~4 to 5% (Ref 2). It is believed that the volume expansion will cause damage to the integrity of the top-coating, which could result in failure during the application of the coating.

X-ray diffraction phase analysis shows the as-sprayed burner cans to consist almost entirely of tetragonal T′ phase. Only traces of monoclinic phase are detected in the structure. Following the quantitative phase analysis described in the experimental details, the monoclinic volume fraction is estimated at 1%. However, large errors are associated with this figure because of the weak peaks associated with the monoclinic phase. Figure 9(a) shows the partial x-ray diagram from BC1 after 35 thermal shock cycles. The large peak in the center of the diagram is the reflection from the (111) tetragonal (T′) planes. The maximum intensity reached 54 counts/s. Only traces of monoclinic phase are found, and the peak positions of the $(11\bar{1})$ and the (111) reflections of the monoclinic phase are indicated in the diagram. Quantitatively, the monoclinic volume fraction is estimated at 1%. No significant phase changes occurred during the 35 thermal shock cycles. Figure 9b shows the corresponding x-ray diagram from BC2 after 1000 thermal shock cycles. The monoclinic peaks are now clearly visible and, quantitatively, the monoclinic volume fraction was estimated to be 3.3%. X-ray diffraction phase analysis from the {400} region ($72° < 2\theta < 76°$) gave no indication of the presence of any cubic phase in the samples.

Brandon and Taylor (Ref 19) studied phase changes during annealing of plasma-sprayed zirconia-yttria mixtures. The decomposition of the T′ phase was found to be sluggish at temperatures below 1300 °C, for zirconia stabilized with 8 wt% yttria. In fact, annealing at 1300 °C for 30 h showed no decomposition of

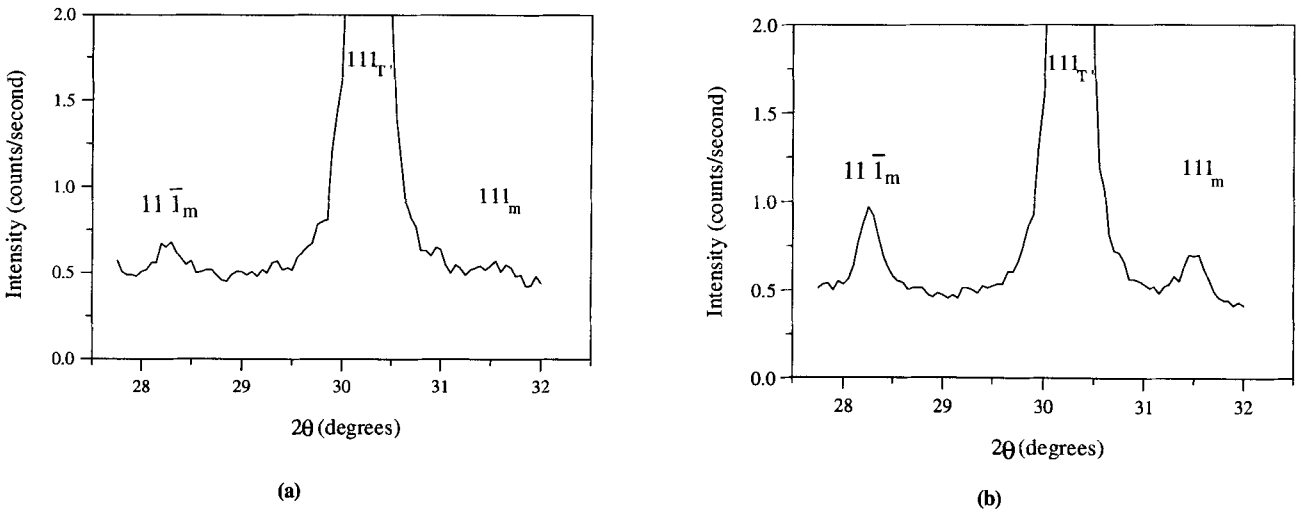

Fig. 9 (a) X-ray diffraction diagrams of the monoclinic and tetragonal reflections from BC1 after 35 thermal shock cycles. Only traces of monoclinic phase are found. (b) X-ray diffraction diagrams of the monoclinic and tetragonal reflections from BC2 after 1000 thermal shock cycles

the T′ phase. At 1400 °C, cubic phase was detected after 3 h. From the present experiment, 1000 thermal shock cycles exposed the burner can to ~20 h at high temperatures. Since the decomposition of the T′ phase has begun, and by comparison with the results of Brandon and Taylor, it is likely that the maximum surface temperature of the top coating reached somewhere between 1300 and 1400 °C during the thermal shock testing. This is in agreement with the estimate from the static heat transfer analysis (Ref 13).

Bond-Coating Oxidation. Another mechanism associated with high-temperature exposure is the oxidation of the bond coating. Figure 10(a) shows the bond-coating cross section of BC2 in the as-sprayed condition. Arrows mark the presence of layers within the bond coating, and from energy dispersive x-ray spectroscopy (EDS), the layers are found to be rich in aluminum. The layers are believed to consist of Al_2O_3, which is consistent with other investigations where alumina is found to be the dominant and initial reaction product (Ref 20, 21). Oxidation of the metal is thought to occur in the plasma flame as well as during the splat-forming phase when the droplets hit the underlying material. No signs of cracking within the bond-coating layers are observed and the thickness of the very thin layer observed at the top-coating/bond-coating interface could not be measured in the scanning electron microscope. Quantitative EDS measurements on the bond coating at positions located outside the alumina layers show the compositions to be the same as the powder specification.

Figure 10(b) shows the bond-coating cross section of BC2 after 1000 thermal shock cycles. From the temperature measurements, it is estimated that the bond coating is exposed to at least 1030 °C for 15 h. A continuous alumina layer has been formed at the interface between the bond coating and the top coating. Also, internal oxidation of the bond coating at interfaces between splats is observed. Cracks, parallel to the plane of the interfaces, are visible in the alumina layers (see the black parts indicated by arrows in Fig. 10b). At the interface between top coating and bond coating, the cracks are situated mainly between the alumina scale and the top coating. Regarding the internal bond coating oxidation, the cracks are situated in the middle of the alumina layers. EDS analysis showed a depletion of aluminum in the remainder of the bond coating. As an average, 5 wt% of aluminum is found, compared to the as-sprayed composition of 12 wt%. The thickness of the alumina scale at the interface between bond coating and top coating, at positions where no cracks were present, was measured as 2 ± 0.5 μm.

The bond-coating cross section of BC1 after 35 thermal shock cycles was also investigated. Both internal bond-coating oxidation and oxidation at the interface between top coating and bond coating were observed. Cracks, similar to those in BC2 after thermal shock testing, were visible, and the thickness of the alumina scale between top coating and bond coating was measured as 0.7 ± 0.1 μm.

The formation of cracks within the alumina layers has two major disadvantages. First, the cracks, together with porosity between the bond-coating splats, provide a path for oxygen transport to the interior of the bond coating. This results in interior bond-coating oxidation and a much faster depletion of aluminum from the bond coating. Maier et al. (Ref 22) studied the degradation of a TBC under thermal cycling conditions. After depletion of aluminum from the bond coating, chromia and NiO began to form. The NiO was formed with a high growth rate, and the growth of NiO into the top-coating was thought to initiate the failure of the top-coating. Second, the cracks formed between the oxide layer and the top-coating can propagate into the top coating (Ref 23). This is believed to be part of the initiation of a horizontal crack which finally causes failure of the TBC.

The extent of internal oxidation within the bond coating implies optimization of the bond-coating spray parameters in order to achieve a denser bond coating.

4. Conclusions

Thermal barrier coatings were sprayed onto two different substrates, including circular substrates with a diameter of 25 mm, and a burner can component. During spraying, a segmentation crack network was created in the ceramic top coating when a high substrate temperature and a high lamella thickness (low gun velocity) were used. The crack network divided the top-

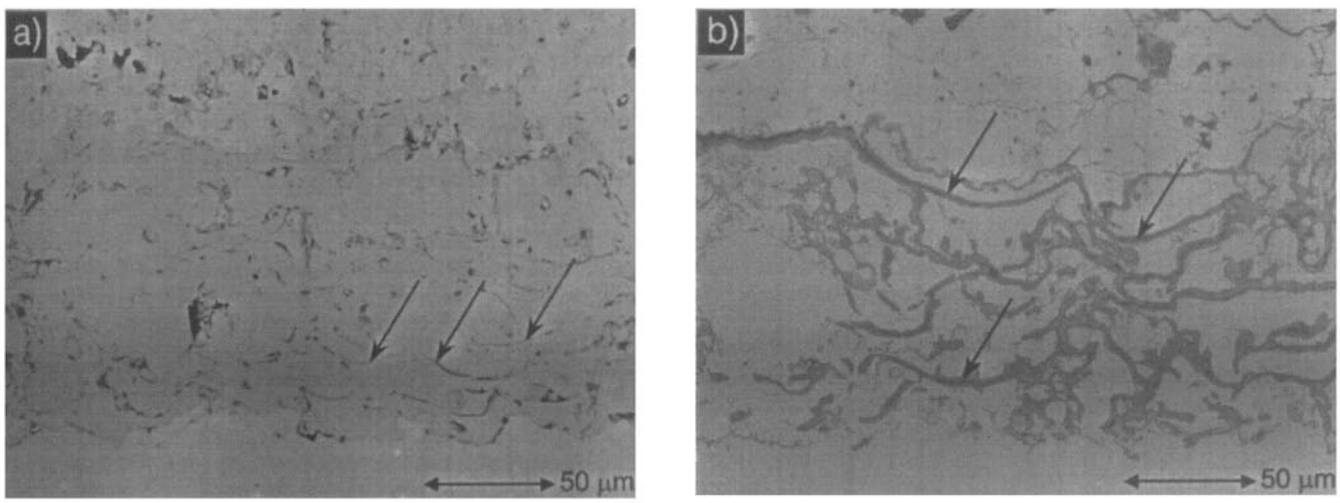

Fig. 10 Polished cross sections of the bond coating in BC2: (a) as-sprayed condition (arrows indicate alumina layers) and (b) after 1000 thermal shock cycles (arrows indicate cracking within the thermally grown alumina)

coating into circular segments, and the measured density of segmentation cracks was found to be independent of the substrate geometry. Consequently, in terms of segmentation cracks, it is possible to apply results from small test samples to real components. Regarding the branching crack lengths, a difference was found between the circular substrates and the burner can. Longer branching cracks were observed in the burner can, and therefore the substrate geometry must be considered before branching crack data are used.

Top coatings sprayed with a low substrate temperature and a low lamella thickness did not contain any segmentation cracks. This was true for both kinds of substrates.

Thermal shock testing of the burner cans showed the segmented burner can to be superior to the nonsegmented burner can. After 1000 thermal shock cycles, the segmentation crack network in the segmented burner can was still stable, and no severe cracks were found within the top coating. In the nonsegmented burner can, a top-coating crack network was found to have been created after only 35 thermal shock cycles. The crack network was much looser compared to the existing segmentation crack network in the segmented burner can. Also, horizontal cracks were found in the top coating at several locations, including the area around the dilution holes. The cracks had propagated in the top coating close to, and sometimes touching, the bond coating. This type of cracking has been shown to cause failure of the TBCs, where the top coating spalls off from the underlying material. Therefore, cracks of this type cannot be tolerated in thick TBCs.

The thermal shock test has shown the segmented burner can to endure the stresses associated with thermal shocks. The failure of the component is believed to be dependent on other time-dependent mechanisms, such as bond-coating oxidation or top-coating decomposition.

Acknowledgments

This work was partially financed by the CEC, contract BRE2-CT94-0936. P. Bengtsson is also grateful for financial support obtained from the Swedish Research Council for Engineering Sciences. The authors thank Jens Dahlin, Volvo Aero Corporation, for carrying out the thermal shock testing.

References

1. T. Khan, Heat-Resistant Materials/Superalloys, *Adv. Mater. Process.*, Vol 1, 1990, p 19-20
2. P.D. Harmsworth and R. Stevens, Phase Composition and Properties of Plasma-Sprayed Zirconia Thermal Barrier Coatings, *J. Mater. Sci.*, Vol 27, 1992, p 611-615
3. G. Johner, V. Wilms, K.K. Schweitzer, and P. Adam, Experimental and Theoretical Aspects of Thick Thermal Barrier Coatings for Turbine Applications, *Thermal Spray: Advances in Coatings Technology*, D.L. Houck, Ed., ASM International, 1988, p 155-166
4. J.E. Nerz, B.A. Kushner, and A.J. Rotolico, Taguchi Analysis of Thick Thermal Barrier Coatings, *Thermal Spray Research and Applications*, T.F. Bernecki, Ed., ASM International, 1991, p 669-673
5. T.A. Taylor, D.L. Appleby, A.E. Weatherill, and J. Griffiths, Plasma-Sprayed Yttria-Stabilized Zirconia Coatings: Structure-Property Relationships, *Surf. Coat. Technol.*, Vol 43/44, 1990, p 470-480
6. T.A. Taylor, Thermal Properties and Microstructure of Two Thermal Barrier Coatings, *Surf. Coat. Technol.*, Vol 54/55, 1992, p 53-57
7. H. Wang, H. Herman, G.A. Bancke, A. Adamski, and M. Wood, Flame Rig Testing of Thick Thermal Barrier Coatings, *Protective Coatings: Processing and Characterization*, R.M. Yazici, Ed., The Minerals, Metals & Materials Society, 1990, p 155-163
8. T.A. Taylor, *Thermal Barrier Coatings for Substrates and Process for Producing it*, U.S. Patent 5,073,433, 17 Dec 1991
9. C. Persson, *Residual Stresses in Metal Matrix Composites after Plastic Straining and Thermal Cycling*, Linköping Studies in Science and Technology, Licentiate Thesis No. 332, 1992
10. H. Toraya, M. Yoshimura, and S. Somiya, Calibration Curve for Quantitative Analysis of the Monoclinic-Tetragonal ZrO_2 System by X-Ray Diffraction, *J. Am. Ceram. Soc.*, Vol 67, 1984, p C119-121
11. H. Toraya, M. Yoshimura, and S. Somiya, Quantitative Analysis of Monoclinic-Stabilized Cubic ZrO_2 Systems by X-Ray Diffraction, *J. Am. Ceram. Soc.*, Vol 67, 1984, p C183-184
12. P. Bengtsson and J. Wigren, Segmentation Cracks in Plasma Sprayed Thick Thermal Barrier Coatings, Materials Solutions '98, 12-15 Oct 98
13. P. Bengtsson, "Determination of Thermal Barrier Coating Thickness for Burner Can Rig Test in BE 7287-3," Technical Report, Reg. No. 9940-062, Volvo Aero Corp., 1994
14. P. Bengtsson, T. Johannesson, and J. Wigren, Crack Structures in Plasma Sprayed Thermal Barrier Coatings as a Function of Deposition Temperature, *Proc. 14th Int. Thermal Spray Conf.*, A. Ohmori, Ed. (Kobe, Japan), May 1995, p 513-518
15. J.H. Sun, E. Chang, C.H. Chao, and M.J. Cheng, The Spalling Modes and Degradation Mechanism of ZrO_2-8 wt.% Y_2O_3/CVD-Al_2O_3/Ni-22Cr-10Al-1Y Thermal-Barrier Coatings, *Oxid. Met.*, Vol 40 (No. 5/6), 1993, p 465-481
16. D. Hull and T.W. Clyne, *An Introduction to Composite Materials*, 2nd ed., Cambridge University Press, 1996
17. H. Scott, Phase Relationships in the Zirconia-Yttria System, *J. Mater. Sci.*, Vol 10, 1975, p 1527-1535
18. R.A. Miller, J.L. Smialek, and R.G. Garlick, Phase Stability in Plasma-Sprayed, Partially Stabilized Zirconia-Yttria, *Int. Conf. on the Sci. and Technol. of Zirconia*, A.H. Heuer and L.W. Hobbs, Ed., 1981, p 241-253
19. J.R. Brandon and R. Taylor, Phase Stability of Zirconia-Based Thermal Barrier Coatings, Part I: Zirconia-Yttria Alloys, *Surf. Coat. Technol.*, Vol 46, 1991, p 75-90
20. L. Lelait, S. Alpérine, and R. Mévrel, Alumina Scale Growth at Zirconia-MCrAlY Interface: A Microstructural Study, *J. Mater. Sci.*, Vol 27, 1992, p 5-12
21. E.Y. Lee, R.R. Biederman, and R.D. Sisson, Diffusional Interactions and Reactions between a Partially Stabilized Zirconia Thermal Barrier Coating and the NiCrAlY Bond Coat, *Mater. Sci. Eng.*, Vol A121, 1989, p 467-473
22. R.D. Maier, C.M. Scheuermann, and C.W. Andrews, Degradation of a Two-Layer Thermal Barrier Coating under Thermal Cycling, *Am. Ceram. Soc. Bull.*, Vol 60 (No. 5), 1981, p 555-560
23. A.H. Bartlett and R. Dal Maschio, Failure Mechanisms of a Zirconia-8 wt% Yttria Thermal Barrier Coating, *J. Am. Ceram. Soc.*, Vol 78 (No. 4), 1995, p 1018-1024